# Journal Pre-proof


Delamination migration in CFRP laminates under mode I loading

Amit Ramji, Yigeng Xu, Mehdi Yasaee, Marzio Grasso, Philip Webb

PII: S0266-3538(19)31791-9

DOI: https://doi.org/10.1016/j.compscitech.2020.108067

Reference: CSTE 108067

To appear in: *Composites Science and Technology*

Received Date: 25 June 2019

Revised Date: 30 December 2019

Accepted Date: 9 February 2020

Please cite this article as: Ramji A, Xu Y, Yasaee M, Grasso M, Webb P, Delamination migration in CFRP laminates under mode I loading, *Composites Science and Technology* (2020), doi: https://doi.org/10.1016/j.compscitech.2020.108067.

Composites Science and Technology, Volume 190, April 2020, Article number 108067
DOI: 10.1016/j.compscitech.2020.108067

# Author Statement

Amit Ramji is the first author responsible for sample preparation and testing, data analysis, and the preparation of the paper.

Yigeng Xu is the corresponding author responsible for setting up the research method and test matrix, results analysis, and the preparation of the paper.

Mehdi Yasaee provides technical support for Amit Ramji in DCB testing, data analysis, and comment for the paper.

Marzio Grasso provides technical support for Amit Ramji on delamination migration analysis and comment for the paper.

Philip Webb provides technical guidance for the research and the preparation of the paper.

**Delamination Migration in CFRP Laminates under Mode I Loading**

Amit Ramji[1], Yigeng Xu[1*], Mehdi Yasaee[1], Marzio Grasso[1], Philip Webb[1]

[1] School of Aerospace, Transport and Manufacturing, Cranfield University, MK43 0AL, UK.

*corresponding author: yigeng.xu@cranfield.ac.uk

**Abstract:** This paper focuses on the effect of interfacial fibre orientation and interleaved veil on the delamination migration of carbon fibre reinforced polymer laminates under Mode I loading. Double cantilever beam specimens with midplane interfacial fibre orientations of 0/0, 90/90, 0/90, 0/45 and 90/45 were tested under two conditions: one with interleaved thermoplastic polyphenylene sulfide veil at the midplane and one without. Results show that, except for the 0/0 configuration, all other orientations exhibit varying levels of migration associated with the interfacial fibre orientation and veil interleaving. The apparent fracture toughness determined with the modified compliance calibration method is closely related to the delamination migration and hence a structural energy dissipation measure dependent on interfacial fibre orientation and the interleaved veil. Distributions of the fibre and matrix materials around the delamination front are found to be closely related to the delamination migration behaviour along its path. The experimental observation and rationalisation presented in this paper provide further knowledge regarding delamination migration and its correlation to the apparent fracture toughness, which is of direct relevance to the damage tolerance design of laminated composite components.

**Keywords**: Delamination – B; Fracture toughness – B; Damage tolerance – C; Fibre bridging – C; Fractography – D

## 1. Introduction

Delamination is often associated with the lack of through-thickness reinforcement and stiffness mismatch between the adjoining layers of a composite laminate. It poses direct threats to the load carrying capacity and service life of laminated composite components. Various methods have been developed to characterize delamination under cyclic or quasi-static loading using linear elastic fracture mechanics theory. The majority of these methods use pre-cracked laminate specimens that grow delamination at a single interface with measurements of the critical strain energy release rate as the fracture toughness of the laminate. This approach has led to several test standards and significant advances towards damage tolerance design and analysis of laminated composite structures [1, 2].

However, practical laminated composite components have multidirectional layup configurations and often involve multisite and interacting damages. Multidirectional carbon fibre reinforced polymer (CFRP) laminates typically exhibit multiple delamination cracks at several interfaces under fatigue load or low velocity impact. Instead of propagating at its initial interface, the delamination may grow through the thickness, joining up with delamination at neighbouring interface or kinking out of the original interface into neighbouring interface on its own. The transition of delamination growth between different interfaces of a composite laminate is known as delamination migration and is commonly observed in notched or bonded composite components under low velocity impact, fatigue or thermal loading. It is closely related to the damage tolerance capacity of laminated composite structures and hence triggers a series of research to understand the governing mechanisms of delamination migrations under various material and loading conditions [3-6]. A test configuration using Single Cantilever Beams (SCB) has been developed by Ratcliff *et al.* [6] for controlling width-wise stable migrations. Under the SCB configuration as shown in Fig.1, the loading and stress conditions change for materials around the delamination front

depending on the relative position of the loading point to the delamination front. Controlled migrations occur along the principal plane where the maximum tensile stress is acting on.

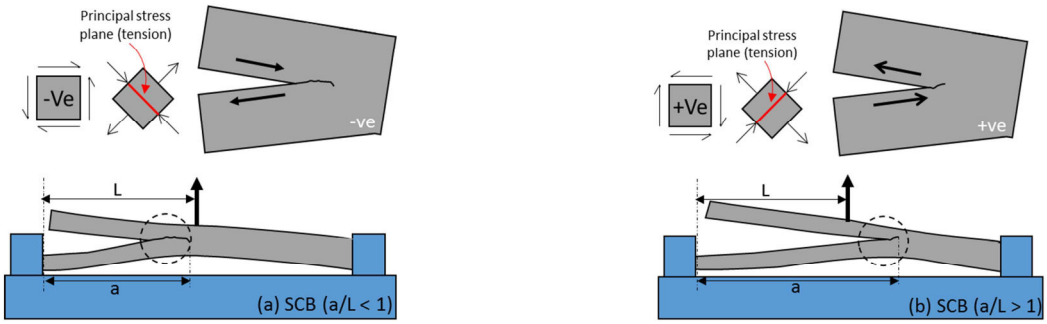


**Fig.1 Stress conditions around the delamination front of the SCB: (a) loading point ahead of the delamination front, (b) loading point behind the delamination front.**

Ratcliff *et al.* [6] demonstrated through the SCB testing of cross-ply CFRP laminates that delamination at the 0/90 interface migrated to a neighbouring 90/0 interface by kinking through the 90° ply stack. The transition from the delamination at the 0/90 interface into the 90° ply stack was gradual whilst the transition of the kinked crack into the 90/0 interface was sudden. These migration behaviours provide valuable experimental evidence in validating analytical and numerical models aimed at predicting delamination migration. Subsequent researches [7-15] have further advanced the knowledge of delamination migration.

It is however worth noting that delamination migration in multidirectional laminates involves complex interactions of the delamination front with surrounding fibre and matrix materials. Most researches in literature focus on the studies of the delamination migration of cross-ply laminates under the SCB test configuration where the loading condition may not be true representations of practical laminated components. Detailed investigation on the influence of a wide range of interfacial fibre orientations on delamination migration is very limited. Moreover, while substantial efforts have been made to characterise the toughening effect of interleaved veils for composite laminates [16-24], little has been done to understand the effect of interleaved veils on delamination migration, especially for the combined effect of interfacial fibre orientation and interleaving. The present work aims to fill the gap through

detailed experimental investigations of double cantilever beam (DCB) specimens with interfacial fibre orientations of 0/0, 90/90, 0/90, 0/45 and 90/45 under two conditions: one with polyphenylene sulfide (PPS) veil interleave at the midplane and one without. Combined effects of interfacial fibre orientation and PPS veil on delamination migration and apparent fracture toughness have been investigated to develop further knowledge for effective damage tolerance design of laminated composite components under Mode I loading.

## 2. Materials and Experimental Procedures

The pre-impregnated CFRP material was supplied by SHD Composites, consisting of UD carbon T300 fibres, with MTC510 toughened epoxy system of 37% resin weight [25]. It has an areal density of 150gm$^{-2}$ and nominal ply cure thickness of 0.15mm with relevant mechanical properties listed in Table 1. Each non-interleaved sample for a specific midplane fibre orientation had a veil interleaved counterpart for comparison. The veils supplied by Technical Fibre Products are Optiveil OP-49-48 [26], with nominal areal density of 10gm$^{-2}$ and thickness of 0.09mm. Veils were manufactured using a wet-lay process with chopped strand PPS fibres of 10μm diameter and length of 6mm in a styrene acrylic binder.

**Table 1 Mechanical properties of *MTC510--UD150-HS-37%RW* [25].**

| **Property** | **Result** | **Standard** |
|---|---|---|
| | | |
| | | |
| | | |
| | | |
| | | |
| | | |
| | | |
| 0° Tensile strength [MPa] | 2112 | BS EN ISO 527-5 |
| 0° Tensile modulus [GPa] | 110 | |
| 0° Poisson's ratio | 0.34 | |
| 90° Tensile strength [MPa] | 54 | |
| 90° Tensile modulus [GPa] | 8.2 | |
| 90° Poisson's ratio | 0.01 | |
| 0° Compression strength [MPa] | 988 | EN 2850 Type B |
| 0° Compression modulus [GPa] | 105.1 | |
| 90° Compression strength [MPa] | 200 | |

| | | |
|---|---|---|
| 90° Compression modulus [GPa] | 9.3 | |
| In-Plane shear strength ± 45° [MPa] | 99 | ASTM D3518 |
| In-Plane shear modulus ± 45° [GPa] | 3.6 | |
| Interlaminar shear strength 0°[MPa] | 85 | BS EN ISO 14130 |

Five specimens were fabricated under the same manufacturing conditions, providing four repetitions for each layup configuration listed in Table 2. The DCB specimens were rectangular with the dimensions of 140(L)×20(B)×4mm(H). For the interleaved configurations, a layer of veil was placed at the midplane, adjacent to the PTFE film insert. The twenty-eight UD CFRP layers were cold consolidated under vacuum during the layup and subsequently placed on a flat steel plate with release film, breather fabric and cured within a vacuum bag in the autoclave. The panels were cured in the autoclave under pressure at 90psig, with a target bag vacuum of 29" Hg (gauge) and temperature set to 100°C for 4 hours as prescribed for MTC510 [25]. The apparent fracture toughness of the specimen was assessed with the modified compliance calibration method as specified in ASTM D5528-13 [27]. The deviation predominantly being the midplane interface configuration, which is required for the study of the effect of fibre orientation and veils on the strain energy release rate and migration mechanisms. Unlike the 0/0 fibre orientation specified in [27], five interfacial fibre orientations as shown in Table 2 were introduced at the midplane of the DCB specimen.



**Table 2 Layup configurations for DCB specimens.**

| Specimen Code | Layup Configuration |
|---|---|
| 90/90 | $[(0, 90)_7]_s$ |
| 90/90 +veil | $[(0, 90)_7, \overline{veil}]_s$ |
| 0/0 | $[(90, 0)_7]_s$ |
| 0/0 +veil | $[(90, 0)_7, \overline{veil}]_s$ |
| 90/0 | $[0, 90]_{14}$ |
| 90/0 +veil | $[(0, 90)_7, \overline{veil}, (0/90)_7]$ |
| 90/45 | $[(0, 90)_6, (-45, 90, 45, 0), (90, 0)_6]$ |
| 90/45 +veil | $[(0, 90)_6, (-45, 90, \overline{veil}, 45, 0), (90, 0)_6]$ |
| 0/45 | $[(90, 0)_6, (-45, 0, 45, 90), (0, 90)_6]$ |
| 0/45 +veil | $[(90, 0)_6, (-45, 0, \overline{veil}, 45, 90), (0, 90)_6]$ |

The specimens were clamped via cyanoacrylate bonded hinges into vice grip fixtures and axially aligned with the load path. A printed scale bar affixed to the specimen allowed visual observation of the delamination front on a white painted edge. The tests were conducted using a 5kN dual column servo-electric universal test machine (Instron 5965). The crosshead displacement rate was set to a constant 2mm/min. The test process was captured on video using a 150mm macro lens and tripod-mounted DSLR camera system shown in Fig.2.

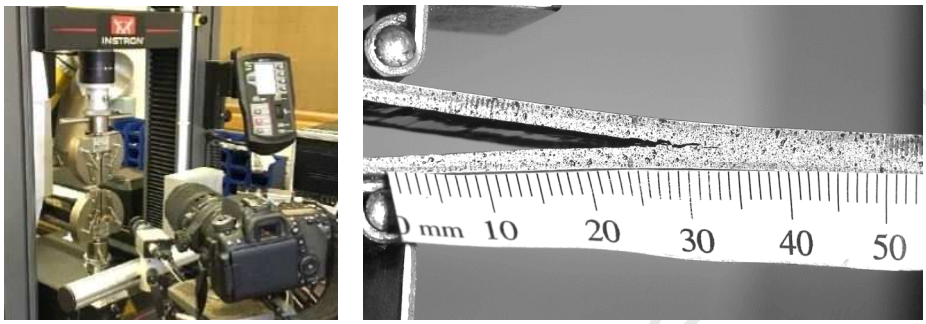


**Fig.2 (a) Test setup, (b) Loaded specimen.**

Fig.2(a) displays the test set-up with Dantec 400 DIC and Fig.2(b) displays the speckle pattern on the edge of the specimen used for the digital image correlation (DIC) analysis. The onset of delamination and subsequent growth were identified by cross-referencing the video recording with the loading rate and the recording time. The resolution of the images is within ±0.5mm which is high enough to deduce the crack tip according to the ASTM standard [27]. The onset of delamination and subsequent growth have been double checked by correlating these events to the sudden load-drops of the load-displacement histories of the specimens in Fig.3.

The specimens were continuously loaded until sufficient data points were obtained or specimen failure. Delamination length measurements were obtained by correlating the video recording with the constant displacement rate. The Mode I strain energy release rates, $G_I$, were then calculated using the modified compliance calibration method [27]:

$$G_I = \frac{3P^2C^{2/3}}{2A_1bh} \quad (1)$$

where $P$ is the applied load. $C$ is the compliance determined by the ratio of the load point displacement to the applied load, δ/P. $A_1$ is the slope of the least squares plot of delamination length normalized by specimen thickness, a/h, as a function of the cube root of compliance, $C^{1/3}$. $b$ is the specimen width and $h$ is the specimen thickness.

## 3. Results

### 3.1. Delamination migration and load-displacement curves

Fig.3 shows the representative load-displacement curves of DCB specimens with five interfacial fibre orientations. Effect of delamination migration is reflected by the change in local slope of the load-displacement curve associated with the intermittent delamination deflection and growth in the migration process. This is supported by the noticeable fluctuations of the load-displacement curves in Fig.3 for all configurations except the 0/0 specimen. Specimens with the 0/0 interfacial fibre orientation do not exhibit significant load fluctuation as the delamination growth is continuous in the absence of delamination migration. The small load fluctuation for the 0/0 specimen is related to localised fibre pull-out, fibre breakage and delamination propagation along the 0/0 interface. Further evidence can be found in the fractographic examination in Section 3.3.

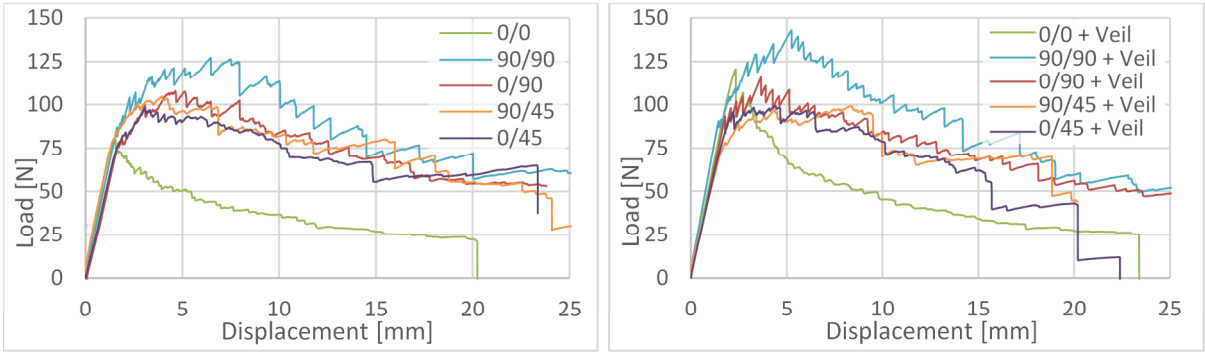


(a) (b)

**Fig.3 DCB Load-displacement curves: (a) without veils, (b) with interleaved veils.**

The load-displacement behaviour of specimens with the veil interleave is shown in Fig.3(b). In comparison to the curves in Fig.3(a), the veil interleave generally improves the resistance to delamination growth. The beneficial effect of the veil is however dependent on the fibre

orientation at the midplane. Specimens with the 0/0 configuration showed the most benefit from the veil, while other midplane orientations appear to receive varying levels of enhancements. Levels of load fluctuations in interleaved specimens are similar to those of specimens without the veil.

### 3.2. Delamination migration and apparent fracture toughness

Fig.4 shows the resistance curves (R-curves) derived from the load-displacement curves of repeated DCB tests using the modified compliance calibration method detailed in [27]. The intermittent nature of the delamination migration leads to large variations in the calculated strain energy release rate ($G_I$) for specimens of 90/90, 0/90, 90/45 and 0/45 interfacial fibre orientations.

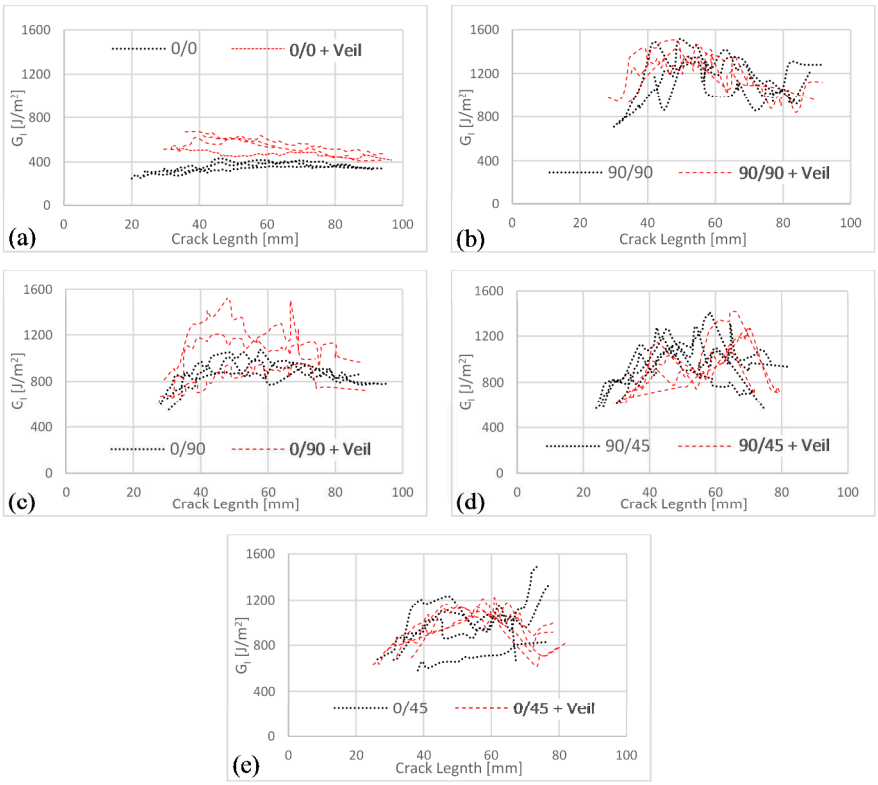


**Fig.4 R-curves with interfacial fibre orientations of: (a) 0/0, (b) 90/90, (c) 0/90, (d) 90/45, and (e) 0/45.**

The 0/0 specimen results (Fig.4(a)) are grouped closely with minimum variation, indicating continuous delamination growth along the 0/0 interface with no delamination migration. The PPS veil has a clear beneficial effect on the fracture resistance at small delamination length

(<80mm). The R-curves for specimens with other four midplane configurations (Figs.4(b)-4(e)) show varying levels of enhancement of fracture resistance, which is related to varying levels of migrations to be detailed in Section 3.3. For the 90/90 configuration (Fig.4(b)), although the R-curves show a small increase in fracture resistance with PPS interleaves, similar large variations of $G_I$ for both veiled and unveiled specimens indicate that delamination migration occurred and the delamination was governed by the same mechanism. R-curves for 0/90 configuration (Fig.4(c)) exhibited noticeable improvement of the veiled specimen over unveiled specimen on fracture resistance at small delamination length. R-curves for 90/45 (Fig.4(d)) configuration show no clear distinction between unveiled and veiled specimens, indicating similar resistance to delamination growth. This is associated with immediate delamination migration at the front of the PTFE film during the test. Instead of propagating along the 90/45 midplane where the veil was added, the initial delamination created by the PTFE film insert tends to migrate immediately into either the 90 layer above or the 45 layer below the midplane interface. This triggers large variations of the fracture resistance shown in Fig.4(d) for this configuration, which is directly related to the delamination migration behaviour to be detailed in Section 3.3.4. The veil therefore has negligible effect on the R-curves of veiled and unveiled 90/45 specimens. R-curves for 0/45 (Fig.4(e)) configuration show a small increase in fracture resistance with PPS interleaves. Section 3.3.5 shows the delamination migration behaviour of 0/45 configuration.

Table 3 summarises test results of delamination resistance of the DCB specimens in terms of strain energy release rate $G_I$. Considering large variations in calculated strain energy release rate due to intermittent delamination migration, mean values of repeated tests for the same specimen configuration over the delamination length between 30mm and 60mm were presented to facilitate the assessment of the overall effect of interfacial fibre orientation and PPS veil on delamination resistance. Results show interfacial fibre orientation has significant

effects on delamination resistance with the 0/0 interface having the lowest toughness. The delamination resistance at the 90/90 interface is 3.2 times of that at the 0/0 interface for specimens without the veil. Thermoplastic veils improve the delamination resistance in general but its improvement is fibre orientation dependent with the 0/0 interface showing the greatest improvement of 41%. Delamination resistance at the 90/90 interface is 2.4 times greater that of the 0/0 interface with the veil. It is however worth noting that only the 0/0 delamination resistance reported in Table 3 represents the fracture toughness $G_{IC}$ for the 0/0 interface. The delamination resistance values for 90/90, 0/90, 90/45 and 0/45 interfaces are not the pure Mode I fracture toughness $G_{IC}$ for these interfaces due to delamination migration. They represent apparent fracture toughness for delamination at these interfaces over the length of 30 – 60mm. The fact that delamination avoids these interfaces indicates that the true $G_{IC}$ values for these interfaces are higher than the apparent fracture toughness shown in the table.

**Table 3 Delamination resistance of DCB specimens.**

| **Midplane** | **Strain energy release rate (No veil) [J/m$^2$]** | | **Strain energy release rate (With veil) [J/m$^2$]** | | **Effect of the veil** |
|---|---|---|---|---|---|
| | **Mean** | **StdDev** | **Mean** | **StdDev** | |
| 0/0 | 369 | 62 | 522 | 63 | +41% |
| 90/90* | 1164 | 163 | 1236 | 141 | +6% |
| 0/90* | 843 | 236 | 974 | 145 | +15% |
| 90/45* | 801 | 184 | 810 | 199 | +1% |
| 0/45* | 746 | 184 | 792 | 182 | +6% |

**Apparent fracture toughness due to delamination migration*

### 3.3. Mechanisms of delamination migration in CFRP laminates

It is expected that delamination migration is influenced by the local stress field around the delamination front. The interfacial fibre orientation and the veil interleave will affect the local stress field and hence the migration behaviour. Upon completion of the DCB tests, optical microscopy was used to characterise the delamination path and fracture surfaces. The

fractographic information is combined with the analysis of the local distribution of fibre reinforcement and epoxy matrix materials around the delamination front to understand the mechanism for delamination migration in multidirectional CFRP laminates.

### 3.3.1. Delamination path for DCB specimen with 0/0 midplane

Fig.5(a) is a representative sideview of the delamination growth path of the DCB specimen with the 0/0 interfacial fibre orientation at the midplane. Stable delamination growth along the 0/0 interface was observed for both the interleaved and non-interleaved specimens, which is expected as the 0° fibre at the interface prevents delamination migration. There is however a clear difference in the morphology of the fracture surfaces between the interleaved and non-interleaved specimens. Compared with the non-interleaved specimen (Fig.5(b)), the veil-interleaved specimen (Fig.5(c)) exhibited a coarser fracture surface with increased fibre pull-out and bridging. These fractographic findings are consistent with the test results in sections 3.1 & 3.2 showing noticeable benefits of PPS veil on delamination resistance. The fracture toughness of the interleaved specimen is 41% higher than that of the non-interleaved specimen (Table 3). The force-displacement curve in Fig.3(a) exhibited an elastic response up to 80 N for non-interleaved specimens whereas veil interleaved 0/0 specimens had a peak force of 120 N as shown in Fig.3(b).

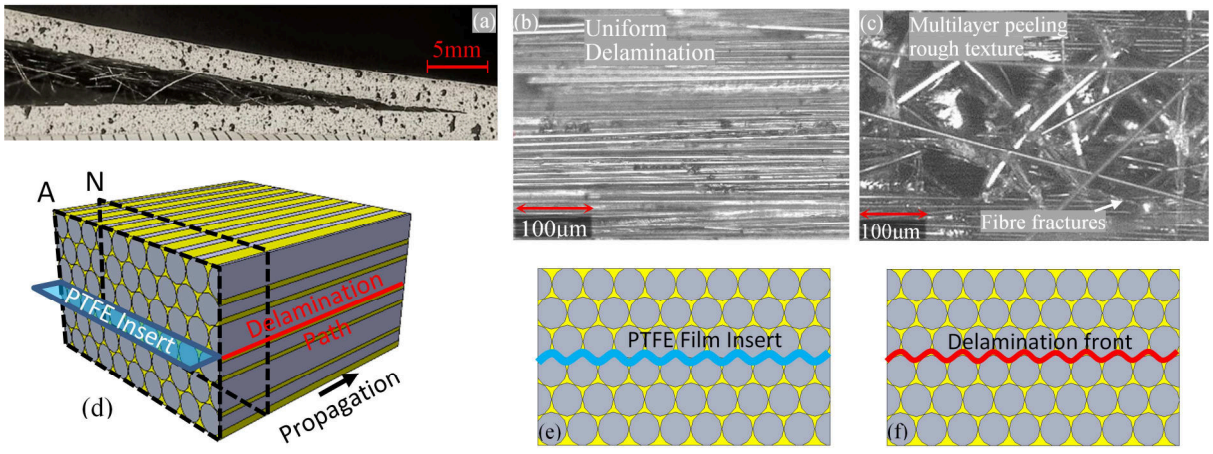

**Fig.5 Delamination path for 0/0: (a) side view, (b) fracture surface without veil, (c) fracture surface with veil, (d) 3D illustration of delamination path, (e) A-A section view, (f) N-N section view.**

Fig.5(d) is the 3D illustration for the distribution of fibre reinforcement (grey) and epoxy matrix material (yellow) along the delamination path (red) of the 0/0 DCB specimen., Delamination migration from the 0/0 midplane interface is prevented due to the existence of reinforcement fibres in the propagation direction. Fig.5(e) is the section view showing the width-wise delamination profile and the distribution of the fibre and matrix materials at the plane where the PTFE insert stops. The actual waviness of the delamination profile is very small considering the diameter (5 – 10 μm) of the carbon fibre and the delamination growth is confined within a narrow rectangular strip (yellow strip on the front face in Fig.5(d)). Fig.5(f) is the section view after the delamination has propagated along the 0/0 interface for some distance. The delamination profile and distribution of the fibre and matrix materials are the same in Fig.5(e) and Fig.5(f), demonstrating the same resistance during delamination growth and rationalising the stable and continuous delamination growth behaviour observed in the 0/0 DCB tests (Fig.3). While multiple delamination damages are commonly observed at separate interfaces above and below the midplane, delamination migration and multi-layer delamination coalescence through the thickness of the laminate cannot occur for 0/0 interleaved and non-interleaved specimens. The dominant failure mode is the interlaminar failure along the 0/0 interface for 0/0 specimens.

### 3.3.2. Delamination path for DCB specimen with 90/90 midplane

Fig.6(a) is a representative sideview of the delamination growth path of the DCB specimen with the 90/90 interfacial fibre orientation at the midplane. Unstable and undulating delamination growth was observed for both the interleaved and non-interleaved specimens, exhibiting the tendency of delamination migration through the thickness of the 90/90 DCB specimen. Localised fibre fracture was observed as the 90° bundles were ‘pulled-out’ from

the laminae matrix and remained partially bonded to each surface. The force-displacement curve in Fig.3 exhibited an elastic response up to 127 N for non-interleaved 90/90 specimens whereas veil interleaved 90/90 specimens had a peak force of 143 N. The 6% increase in apparent fracture toughness shown in Table 3 for veil-interleaved 90/90 specimens can be attributed to the enhanced fibre pull-out and bridging of the veiled interleaved specimen (Fig.6(c)) compared with the non-interleaved specimen (Fig.6(b)).

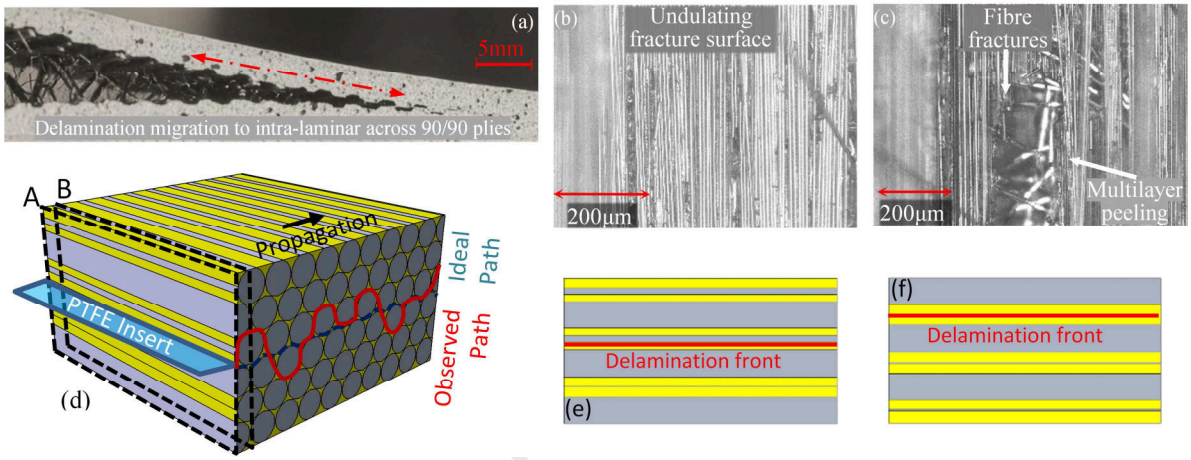


**Fig.6 Delamination path for 90/90: (a) side view, (b) fracture surface without veil, (c) fracture surface with veil, (d) 3D illustration of delamination path, (e) A-A section view, (f) B-B section view.**

Fig.6(d) is the 3D illustration for the distribution of fibre reinforcement and matrix materials along the delamination path of the 90/90 DCB specimen. Fig.6(e) is the section view showing the through-thickness distribution of the fibre and matrix materials at the A-A plane. Fig.6(f) is the section view after the delamination has propagated to the B-B plane. There is a clear difference in local distribution of fibre and matrix materials between planes A-A and B-B, affecting the local stress field around the delamination front and hence the delamination resistance (Fig.3). It is expected that the resin rich regions are prone to the initiation and coalescence of micro matrix cracks and hence trigger delamination deflection and migration. The migration path in Fig.6(d) is determined based on the analysis of the variations of the resin rich regions around the delamination front and test observations (Fig.6(a)). Migration from the 90/90 midplane is frequently accompanied with direction changes, reverting towards

the midplane where the maximum applied stress exists under mode I loading. As a result, the delamination will propagate along the observed undulating red path, not along the ideal blue path at the 90/90 midplane interface shown in Fig.6(d). The delamination migration introduces mixed mode delamination growth and reduces the effective driving force due to delamination deflection. The delamination resistance measured from the 90/90 DCB specimen is therefore the apparent fracture toughness and is considerably higher than that of the 0/0 DCB specimen (Table 3). The dominant failure mechanism for 90/90 interleaved and non-interleaved DCB specimens is intra-laminar failure.

### 3.3.3. Delamination path for DCB specimen with 0/90 midplane

Fig.7(a) is a representative sideview of the delamination growth path of the DCB specimen with the 0/90 interfacial fibre orientation at the midplane. Similar to the observation of 90/90 specimens, delamination growth is unstable but the level of undulation is less significant in 0/90 as the delamination strays within a single 90° lamina. It was observed across the repeated tests that the delamination migrated into the 90° layer after the PTFE insert, demonstrating that the neighbouring 90° intra-laminar interface was weaker than the 0/90 interface and the measured delamination resistance in Table 3 is the apparent fracture toughness of the 0/90 DCB specimen. The force-displacement curve exhibited an elastic response up to 105 N for non-interleaved 0/90 specimens (Fig.3(a)), whereas veil interleaved 0/90 specimens had a peak elastic load limit of 115 N (Fig.3(b)). The fracture surface for the interleaved midplane (Fig.7(c)) was coarser and irregular compared to the non-interleaved midplane (Fig.7(b)). The difference in the elastic load limit and fracture surface morphology between non-interleaved and interleaved specimens contributing to 15% improvement in apparent fracture toughness (Table 3)..,

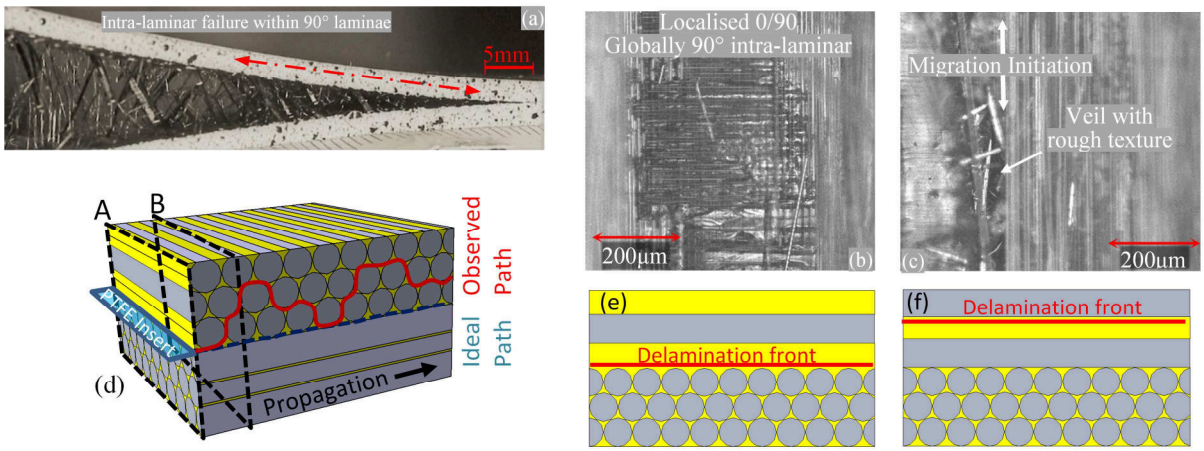


**Fig.7 Delamination path for 0/90: (a) side view, (b) fracture surface without veil, (c) fracture surface with veil, (d) 3D illustration of delamination path, (e) A-A section view, (f) B-B section view.**

Fig.7(d) is the 3D illustration for the distribution of fibre reinforcement and matrix materials along the delamination path of the 0/90 DCB specimen. Fig.7(e) is the section view showing the through-thickness distribution of the fibre and matrix material at the A-A plane. Fig.7(f) is the section view after the delamination has propagated to the B-B plane. Similar to the 90/90 interfaces, clear difference in local distribution of fibre and matrix exists between planes A-A and B-B, indicating differences in the local stress field around the delamination front and hence the resistance to delamination growth (Fig.3). The delamination tends to deflect into the resin rich area and migrate into the 90° layer, not into the 0° laminae due to the strong 0° fibres at the interface. The delamination resistance measured from the 0/90 DCB specimen is therefore the apparent fracture toughness and is much higher than that of the 0/0 DCB specimen (Table 3) due to delamination migration. The dominant failure mechanism for 0/90 interleaved and non-interleaved DCB specimens is intra-laminar failure of the 90° layer.

### 3.3.4. Delamination path for DCB specimen with 90/45 midplane

Fig.8(a) is a representative sideview of the delamination growth path of the DCB specimen with the 90/45 interfacial fibre orientation at the midplane. Delamination propagated mainly

within the 45° laminae for both non-interleaved and interleaved specimens, not along the pre-cracked 90/45 interface. Fig.8(a) shows a region (9~10mm) where intra-laminar migration into the 90° laminae is observed. Migration into the 90° laminae occurred after the initial 45° fibres ended at the rear edge of the specimens. Chen *et al.* [11]and Gong *et al.* [14,15] describes the width-wise delamination being non-uniform due to the ply-splits when considering 45° laminae. Similar large-scale migrations were observed across all repetitions for non-interleaved and veil interleaved 90/45 specimens. Fracture features similar to the 0/90 mid-planes were observed (Figs.8(b-c)), indicating the influence of neighbouring laminae on the apparent fracture toughness. The small difference (1%) in the load limit (Fig.3) and apparent fracture toughness (Table 3) for non-interleaved and interleaved 90/45 midplanes shows a negligible effect of the veil due to immediate delamination migration which makes the delamination not to propagate along the pre-cracked 90/45 interface where the veil was inserted.

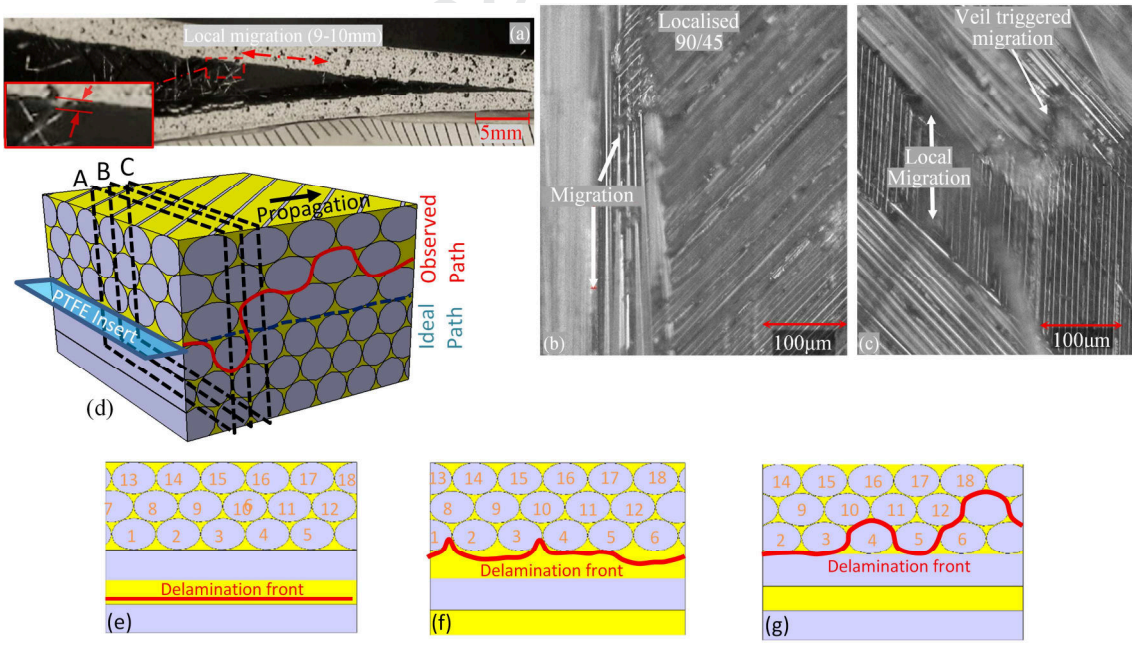


**Fig.8 Delamination path for 90/45 specimen: (a) side view, (b) fracture surface without veil, (c) fracture surface with veil, (d) 3D illustration of delamination path, (e) A-A section view, (f) B-B section view, (g) C-C section view.**

Fig.8(d) is the 3D illustration for the distribution of fibre reinforcement and matrix materials along the delamination path of the 90/45 DCB specimen. Figs.8(e-g) are the section views showing the through-thickness distribution of the fibre and matrix material and the profiles of the delamination front at planes of A-A, B-B, and C-C, respectively. The distribution of fibre and matrix materials varies from plane to plane along the delamination path, which triggers delamination migration and affect the resistance to delamination shown in Fig.3 and Table 3. The dominant failure mechanism for 90/45 midplane specimens for interleaved and non-interleaved was intra-laminar failure of the 45° and 90° layers. Unlike the 0/0, 90/90, 0/90 specimens, the delamination front across the width of the 90/45 DCB specimen is no longer uniform. Instead, the delamination front was skewed across the width of the specimen as shown in Fig.8(g), which could be linked to the presence of the 45° ply splits in the 90/45 specimen [11,14,15]. It is however worth noting that the profile in Fig.8(g) only represents one of the many possible outcomes, factors such as local misalignment of fibres or defects may trigger migrations at different locations and hence lead to different delamination front profiles. Further investigation is required to understand the effect of 45° layer on the profile of the delamination front.



### 3.3.5. Delamination path for DCB specimen with 0/45 midplane

Fig.9(a) is a representative sideview of the delamination growth path of the DCB specimen with the 0/45 interfacial fibre orientation at the midplane. It was observed that intra-laminar failure first occurred within the 45° laminae, then progressed through a combination of 45° and 90° plies as intra-laminar failure from ~25mm to ~40mm, and finally propagated through the neighbouring 90° until ~64mm from the hinge pin. The 6% increase in apparent fracture toughness shown in Table 3 for veil-interleaved 0/45 specimens can be attributed to the enhanced fibre bridging and the veil triggered migration of the interleaved specimen (Fig.9(c)) compared with the non-interleaved specimen (Fig.9(b)).

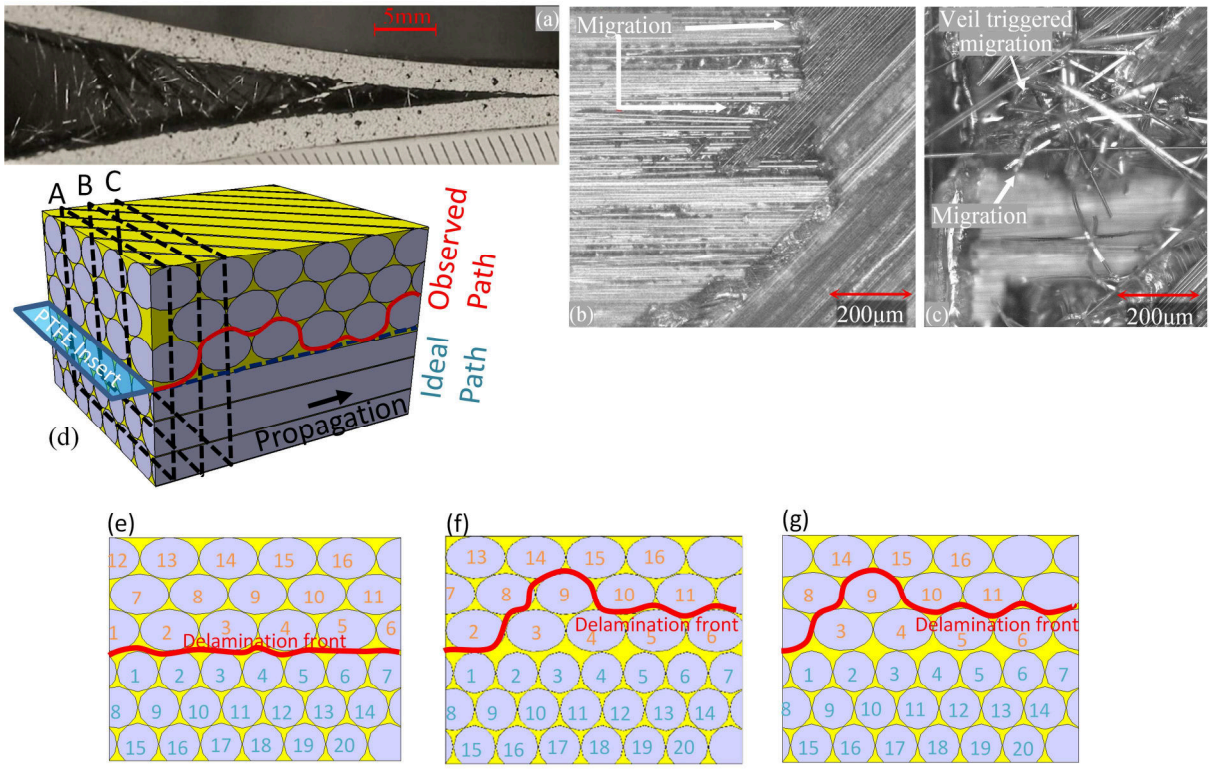


**Fig.9 Delamination path for 0/45 specimen: (a) side view, (b) fracture surface without veil, (c) fracture surface with veil, (d) 3D illustration of delamination path, (e) A-A section view, (f) B-B section view, (g) C-C section view.**

Fig.9(d) is the 3D illustration for the distribution of fibre reinforcement and matrix materials along the delamination path of the 0/45 DCB specimen. Figs.9(e-g) are the section views showing the through-thickness distribution of the fibre and matrix materials and the profiles of the delamination front at planes A-A, B-B, and C-C, respectively. Similar to what was observed for 90/45 specimens, the dominant failure mechanism for 0/45 specimens for interleaved and non-interleaved was intra-laminar failure of the 45° and neighbouring 90° layers. The delamination front of the 0/45 DCB specimen was skewed across the width of the specimen as shown in Figs.9(f-g) due to the presence of 45° fibre splits.

## 4. Discussions

Results of DCB tests show clear tendencies of delamination migration in multidirectional CFRP laminates. Apart from the 0/0 specimens where the delamination propagates along the midplane interface, the remaining four (90/90, 0/90, 90/45, 0/45) specimen configurations

exhibit complex fracture morphologies and delamination paths due to delamination migration (Figs.6-9). The delamination profile is directly related to the interfacial fibre orientation at the midplane. The 90/90 and 0/90 specimens exhibit undulating delamination paths in the lengthwise direction but the delamination front in the width direction is uniform (Figs.6-7). The profiles of the delamination front of the 90/45 and 0/45 specimens were however skewed across the width of the specimen as shown in Figs.8-9, which are related to the presence of ply-splits of the 45° layer [11,14,15]. The bending-twisting coupling due to the inclusion of the 45° layer for the 90/45 and 0/45 configurations is an important aspect to check and may add further complexity to the delamination process. It is however worth noting that the unsymmetrical layup is the necessity to investigate the effect of interfacial fibre orientation on delamination resistance at the 90/45 and 0/45 interfaces in the current study. Moreover, it is expected that the effect of the bending-twisting coupling on the global behaviour of the specimen is insignificant due to the fact that the four unsymmetrical layers were confined to the midplane and constrained by dominant outside twenty-four symmetric cross-ply layers as shown in Table 2. This is supported by the experimental observation that the rotation in 90/45 and 0/45 specimens was negligible during the DCB testing. Finite element simulation is being carried out to quantify the effect of the 45° layer with preliminary results showing very small (<3%) mode II and mode III elements during delamination growth for the DCB specimens of 90/45 and 0/45 configurations. Details of the FE model and the numerical results will be presented in another paper focusing on the quantification of the bending-twisting coupling effect and the variation of the delamination resistance.

Delamination migration leads to the stick slip delamination growth behaviour and contributes to the fluctuations of loads in Fig.3 and significant variations of the delamination resistance in Fig.4. The strain energy release rate measured for the specimens of interfacial fibre orientations other than 0/0 is the apparent fracture toughness representing averaged resistance

to delamination growth, not the mode I fracture toughness $G_{IC}$ value for the resistance to delamination growth along the interface. The 3D profile of the delamination surface and enhanced fibre bridging and breakage due to delamination migration lead to improved resistance to delamination growth of 90/90, 0/90, 90/45 and 0/45 specimens in comparison to the 0/0 specimen. The apparent fracture toughness of the 90/90 specimen is 3.2 times of that at the 0/0 interface for specimens without the veil. Therefore, ASTM 5528-13 [27] provides a conservative approach in suggesting the use of 0/0 DCB specimen to derive the $G_{IC}$ of the composite laminate for engineering application but can be overly conservative in design optimisation for weight saving. Veil interleaving is considered as an established method for improving the fracture toughness of multidirectional CFRP laminates [16-24]. DCB test results (Table 3) in the current study show that PPS veil led to enhanced fibre bridging and fibre breakage (Figs.5-9) and hence improved the resistance to delamination growth. The improvement on the apparent fracture toughness is however fibre orientation dependent, varying from 41% for the 0/0 specimen to 1% for the 90/45 specimen. Considering that most studies on the effect of interleaving has been conducted on 0/0 DCB specimens [16-24], toughening effect of interleaving veils could be over-projected and incorrectly prescribed for multidirectional CFRP laminates. DCB test results in Table 3 also show that interfacial fibre orientation has dominant influence on delamination resistance but the influence is reduced with the addition of the PPS veil. For specimens with the veil interleave, apparent fracture toughness of the 90/90 specimens is 2.4 times that of the 0/0 specimen, which is less than 3.2 times for specimens without the veil. It is also worth noting that the effect of interleaving veil on apparent fracture toughness exists after the delamination has migrated away from the veiled interface, indicating that the PPS veil may affect not only the material at the interface but also the neighbouring materials.

The effect of interfacial fibre orientation and interleaving veil on apparent fracture toughness is clearly linked to delamination migrations. A good understanding of migration mechanisms is essential yet challenging to exploit the full potential of multidirectional CFRP laminates. This has been illustrated in Figs.6-9 showing complex delamination migration paths in multidirectional CFRP laminates under the influence of many factors. Ratcliff *et al.* [6-8] argued that delamination migrated along the plane under the principal tensile stress (Fig.1) and demonstrated that the migration path could be predicted by correlating the applied load to the stress field near the delamination front. It is however worth noting that the test configuration in the study of Ratcliff *et al.* [6-8] is specifically developed for controlling width-wise and stable migrations. The loading condition and stress state around the delamination front changes with the relative position of the loading point to the delamination front as illustrated in Fig.1. Delamination migration behaviours observed in the SCB testing hence may not be representative for multidirectional CFRP laminates under mode I loading. Moreover, the correlation between the applied load and the stress field in Fig.1 does not account for highly anisotropic natures of multidirectional CFRP laminates and cannot rationalize the dominant influence of interfacial fibre orientations on delamination migration and fracture toughness. It is expected that the resin rich regions are the weak areas for the initiation and coalescence of micro matrix cracks to trigger delamination deflection and migration. Detailed analyses of the variations in local distribution of fibre and matrix materials around the delamination front in the current study (Figs.6-9) offer a meaningful and effective approach to predict delamination migration path in multidirectional CFRP laminates, which will help to develop reliable design and simulation tools for the prediction of mechanical performance of laminated composite structures. Further research is being carried out to develop an effective predictive model for the delamination migration based on the understanding of migration mechanisms. Outcome of the research will be presented in

another paper together with the quantification of the bending-twisting coupling effect and the variation of the delamination resistance.

It is worth noting that the apparent fracture toughness for a specific DCB configuration in Table 3 is a structural energy dissipation measure of the specific coupon, not a material property for the resistance to delamination propagation at the midplane. This is due to the delamination migration and enhanced fibre bridging in the wake of delamination front, making the measured apparent fracture toughness delamination length dependent. The apparent fracture toughness in Table 3 represents averaged strain energy release rate over the delamination length of 30 – 60mm for a given DCB configuration and is determined with the modified compliance calibration method which is suitable for unidirectional laminates but may not be accurate for measuring the strain energy release rate for multidirectional laminate. For the layups with the 45° ply around the midplane, the delamination front was skewed, which means that the local features of the apparent delamination path are comparable in size to the dimensions of the specimen and are not free of boundary effects. The apparent fracture toughness values in Table 3 are hence not true material properties and shouldn't be directly used for design and modelling of a generic multidirectional composite structure. Nevertheless, the findings reported in the current study represent reliable test data based on repeated tests of multiple specimens of the same material and geometry under the same testing conditions. They are valid for a comparison study of the effect of interfacial fibre orientation and interleaving veil on delamination migration and delamination resistance, which is the focus of the current study and is essential for the development of advanced design and simulation tools for reliable damage tolerance analysis of laminated composite structures. Further research is however required to quantify the effect of above issues so that converged design parameters free of boundary effects can be determined for given interfaces in the design and analysis of a generic composite structure.

## 5. Conclusions

Effects of interfacial fibre orientation and interleaved PPS veils on delamination migration and delamination resistance have been investigated for CFRP laminates under mode I loading. Following conclusions can be drawn from the findings in the study:

- Delamination migration takes place when interfacial fibre orientations have element of 90° or 45°. The 3D delamination profile and enhanced fibre bridging and breakage due to delamination migration lead to improved resistance to delamination growth of 90/90, 0/90, 90/45 and 0/45 specimens in comparison to the 0/0 specimen. Strain energy release rate value derived based on the modified compliance calibration method in ASTM 5528-13 can be overly conservative in design optimisation for weight saving.
- PPS veils improves the apparent fracture toughness in general but the improvement is fibre orientation dependent, varying from 41% for the 0/0 specimen to 1% for the 90/45 specimen. Toughening effect of interleaving veils assessed with the 0/0 DCB specimen could be over-projected and incorrectly prescribed for multidirectional CFRP laminates. Effect of interleaving veil on apparent fracture toughness exists after the delamination has migrated away from the veiled interface, indicating that the PPS veil may affect not only the material at the interface but also the neighbouring materials.
- Delamination migration has been found to be closely linked to the distributions of the fibre and matrix materials around the delamination front. The observation that delamination path can be predicted based on the analysis of resin rich regions offers a meaningful and effective approach to rationalise the effect of interfacial fibre orientation and interleaving veil on delamination migration and fracture toughness of multidirectional CFRP laminates, which will help to develop advanced design and simulation tools for reliable damage tolerance analysis of laminated composite structures. Further research is

being carried out to develop an effective predictive model for the delamination migration based on the understanding of migration mechanisms.

- The apparent fracture toughness values presented in the paper provide meaningful comparison for the effect of interfacial fibre orientation and interleaving veil on delamination migration and delamination resistance, which is fundamental for the design optimization of composite laminates. They are however not free of boundary effects and are delamination length dependent. As such, they are structural energy dissipation measures for specific specimen configurations and hence not true material properties. Further research is required to determine converged design parameters free of boundary effects for reliable damage tolerance design and analysis of a generic composite structure.

**Acknowledgments**

The authors would like to thank Technical Fibre Products for supplying the Optiveil PPS veils for the investigation. The authors would also like to thank Jim Hurley and Jarryd Braithwaite for their assistance in specimen manufacture and testing. Amit Ramji would like to acknowledge the PhD studentship awarded by SATM at Cranfield University for the study.



**References**

[1] Robinson P, Song DQ. A modified DCB specimen for mode I testing of multidirectional laminates, J Compos Mater 1992; 26: 1554-77.

[2] Andersons J, König M. Dependence of fracture toughness of composite laminates on interface ply orientations and delamination growth direction, Compos Sci Technol 2004; 64: 2139–52.

[3] Greenhalgh ES, Rogers C, Robinson P. Fractographic observations on delamination growth and the subsequent migration through the laminate, Compos Sci Technol 2009; 69: 2345–51.

[4] Canturri C, Greenhalgh ES, Pinho ST, Ankersen J. Delamination growth directionality and the subsequent migration processes – The key to damage tolerant design, Compos Part A 2013; 54: 79–87.

[5] Hallett SR, Green BG, Jiang WG, Wisnom MR. An experimental and numerical investigation into the damage mechanisms in notched composites, Compos Part A 2009; 40: 613–24.

[6] Ratcliffe JG, Czabaj MW, Brien TKO. A test for characterizing delamination migration in carbon / epoxy tape laminates, NASA-Technical-Report TM 218028 A 2013; 1–24.

[7] Pernice FM, De Carvalho NV, Ratcliffe JG, Hallett SR. Experimental study on delamination migration in composite laminates, Compos Part A 2015; 73: 20–34.

[8] De Carvalho NV, Chen BY, Pinho ST, Ratcliffe JG, Baiz PM, Tay TE. Modeling delamination migration in cross-ply tape laminates, Compos Part A 2015; 71: 192–203.

[9] Zhao M, Benedictus R, Jia L, Lyu X, Yao L, Sun Y, Guo L, Alderliesten RC. Mode-I fatigue delamination growth with fibre bridging in multidirectional composite laminates, Eng Fract Mech 2017; 189: 221–31.

[10] Gong Y, Zhao L, Zhang J, Wang Y, Hu N. Delamination propagation criterion including the effect of fiber bridging for mixed-mode I/II delamination in CFRP multidirectional laminates, Compos Sci Technol 2017; 151: 302–9.

[11] Chen BY, Tay TE, Pinho ST, Tan VBC. Modelling delamination migration in angle-ply laminates, Compos Sci Technol 2017; 142: 145–55.

[12] Bin Mohamed Rehan MS, Rousseau J, Fontaine S, Gong XJ. Experimental study of the influence of ply orientation on DCB mode-I delamination behavior by using multidirectional fully isotropic carbon/epoxy laminates, Compos Struct 2017; 161: 1–7.

[13] Samborski S. Prediction of delamination front's advancement direction in the CFRP laminates with mechanical couplings subjected to different fracture toughness tests, Compos Struct 2018; 202: 643–50.

[14] Gong Y, Zhang B, Mukhopadhyay S, Hallett SR. Experimental study on delamination migration in multidirectional laminates under mode II static and fatigue loading, with comparison to mode I, Compos Struct 2018; 201: 683–98.

[15] Gong Y, Zhang B, Hallett SR. Delamination migration in multidirectional composite laminates under mode I quasi-static and fatigue loading, Compos Struct 2018; 189: 160–76.

[16] Nash NH, Young TM, Stanley WF. An investigation of the damage tolerance of carbon/Benzoxazine composites with a thermoplastic toughening interlayer, Compos Struct 2016; 147: 25–32.

[17] Ramirez VA, Hogg PJ, Sampson WW. The influence of the nonwoven veil architectures on interlaminar fracture toughness of interleaved composites, Compos Sci Technol 2015;

110: 103–10.

[18] Daelemans L, van der Heijden S, De Baere I, Rahier H, Van Paepegem W, De Clerck K. Nanofibre bridging as a toughening mechanism in carbon/epoxy composite laminates interleaved with electrospun polyamide nanofibrous veils, Compos Sci Technol 2015; 117: 244–56.

[19] Beckermann GW, Pickering KL. Mode I and Mode-II interlaminar fracture toughness of composite laminates interleaved with electrospun nanofibre veils, Compos Part A 2015; 72: 11–21.

[20] Hogg PJ. Toughening of thermosetting composites with thermoplastic fibres, Mater. Sci. Eng. A 2005; 412: 97–103.

[21] Czabaj MW, Ratcliffe JG. Comparison of intralaminar and interlaminar mode I fracture toughness of unidirectional IM7/8552 graphite/epoxy composite, Compos Sci Technol 2013; 89: 15-23.

[22] Yasaee M, Bond IP, Trask RS, Greenhalgh ES. Damage control using discrete thermoplastic film inserts, Compos Part A 2012; 43: 978–89.

[23] Yasaee M, Bond IP, Trask RS, Greenhalgh ES. Mode II interfacial toughening through discontinuous interleaves for damage suppression and control, Compos Part A 2012; 43: 121–8.

[24] Yasaee M, Bond IP, Trask RS, Greenhalgh ES. Mode I interfacial toughening through discontinuous interleaves for damage suppression and control, Compos Part A 2012; 43: 198–207.

[25] Mechanical properties of MTC510 epoxy UD component prepreg, SHD Composite Materials Ltd (accessed on 11/03/2019, updated on 20/12/2019).

[26] TFP, Opti veil ® OP-49-48-PPS Technical Datasheet, (2015) 1–2. http://www.tfpglobal.com/materials/thermoplastic/OP-49-48-PPS (accessed 02/03/2019).

[27] Standard test method for mode I interlaminar fracture toughness of unidirectional fiber-reinforced polymer matrix composites, ASTM D5528-13 2013; 1–13.

Fig.1 Stress conditions around the delamination front of the SCB: (a) loading point ahead of the delamination front, (b) loading point behind the delamination front.

Fig.2 (a) Test setup, (b) Loaded specimen.

Fig.3 DCB Load-displacement curves: (a) without veils, (b) with interleaved veils.

Fig.4 R-curves with interfacial fibre orientations of: (a) 0/0, (b) 90/90, (c) 0/90, (d) 90/45, and (e) 0/45.

Fig.5 Delamination path for 0/0: (a) side view, (b) fracture surface without veil, (c) fracture surface with veil, (d) 3D illustration of delamination path, (e) A-A section view, (f) N-N section view.

Fig.6 Delamination path for 90/90: (a) side view, (b) fracture surface without veil, (c) fracture surface with veil, (d) 3D illustration of delamination path, (e) A-A section view, (f) B-B section view.

Fig.7 Delamination path for 0/90: (a) side view, (b) fracture surface without veil, (c) fracture surface with veil, (d) 3D illustration of delamination path, (e) A-A section view, (f) B-B section view.

Fig.8 Delamination path for 90/45 specimen: (a) side view, (b) fracture surface without veil, (c) fracture surface with veil, (d) 3D illustration of delamination path, (e) A-A section view, (f) B-B section view, (g) C-C section view.

Fig.9 Delamination path for 0/45 specimen: (a) side view, (b) fracture surface without veil, (c) fracture surface with veil, (d) 3D illustration of delamination path, (e) A-A section view, (f) B-B section view, (g) C-C section view.

# Conflict of Interest Form

Declarations of interest: none

# Delamination migration in CFRP laminates under mode I loading

Ramji, Amit

2020-02-10



Ramji A, Xu Y, Yasaee M, et al., (2020) Delamination migration in CFRP laminates under mode I loading. Composites Science and Technology, Volume 190, April 2020, Article number 108067
https://doi.org/10.1016/j.compscitech.2020.108067